APL Materials

RESEARCH ARTICLE | MARCH 05 2024

Dielectric multilayers impact on radiation-induced charge accumulation in highly sensitive oxide field effect transistors

Camilla Bordoni ; Andrea Ciavatti ; Mariana Cortinhal ; Maria Pereira ; Tobias Cramer ; Pedro Barquinha ; Beatrice Fraboni

APL Mater. 12, 031106 (2024)
https://doi.org/10.1063/5.0189167

CrossMark

06 March 2024 11:31:13

APL Materials ARTICLE pubs.aip.org/aip/apm

Dielectric multilayers impact on radiation-induced charge accumulation in highly sensitive oxide field effect transistors

Cite as: APL Mater. 12, 031106 (2024); doi: 10.1063/5.0189167
Submitted: 27 November 2023 • Accepted: 5 February 2024 •
Published Online: 5 March 2024

View Online

Export Citation
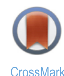
CrossMark

Camilla Bordoni,[1] Andrea Ciavatti,[1,a)] Mariana Cortinhal,[2] Maria Pereira,[2] Tobias Cramer,[1]
Pedro Barquinha,[2] and Beatrice Fraboni[1]

AFFILIATIONS

[1] Department of Physics and Astronomy, University of Bologna, Viale Berti Pichat 6/2, Bologna 40127, Italy
[2] CENIMAT|i3N, Department of Materials Science, NOVA University of Lisbon and CEMOP/UNINOVA, Campus da Caparica, 2829-516 Caparica, Portugal

[a)] Author to whom correspondence should be addressed: andrea.ciavatti2@unibo.it

ABSTRACT

Radiation dosimetry is crucial in many fields where the exposure to ionizing radiation must be precisely controlled to avoid health and environmental safety issues. Among solid state detectors, we recently demonstrated that Radiation sensitive OXide Field Effect Transistors (ROXFETs) are excellent candidates for personal dosimetry thanks to their fast response and high sensitivity to x rays. These transistors use indium–gallium–zinc oxide as a semiconductor, combined with a dielectric based on high-permittivity and high-atomic number materials. Here, we present a study on the ROXFET gate dielectric fabricated by atomic layer deposition, where we compare single- and multi-layer structures to determine the best-performing configuration. All the devices show stable operational parameters and high reproducibility among different detectors. We identified an optimized bi-layer dielectric structure made of tantalum oxide and aluminum oxide, which demonstrated a sensitivity of (63 ± 2) V/Gy, an order of magnitude larger than previously reported values. To explain our findings, we propose a model identifying the relevant charge accumulation and recombination processes leading to the large observed transistor threshold voltage shift under ionizing radiation, i.e., of the parameter that directly defines the sensitivity of the device.

© 2024 Author(s). All article content, except where otherwise noted, is licensed under a Creative Commons Attribution (CC BY) license (http://creativecommons.org/licenses/by/4.0/). https://doi.org/10.1063/5.0189167

06 March 2024 11:31:13

INTRODUCTION

Radiotherapy and radioprotection require accurate monitoring of ionizing radiation exposure in the human body to ensure safety.[1–3] Efficient personal dosimetry requests wearable detectors for continuous monitoring with fast reading, high sensitivity, and possibly wireless data acquisition.[4–6] Other important features are dose rate and radiation energy independence. Solid-state dosimeters are suitable candidates and, among them, Radiation Sensitive Field Effect Transistors (RADFETs) offer easy and real-time reading, lightweight, and low bias or passive operation.[7] Their working principle relies on the accumulation of radiation-generated charges in the gate dielectric, which results in a shift of transistor threshold voltage (V_{th}) toward more negative values proportional to the dose deposited onto the device.[8,9] The radiation sensitivity of the device is proportional to the gate dielectric thickness squared.[10] Modern RADFETs are able to provide 0.25 V/Gy of sensitivity at a standard SiO_2 thickness and up to 0.7V/Gy for thick oxides for MV irradiation while, due to the energy dependence of RADFETs, they can achieve ~5 V/Gy at 35 keV x-ray.[11,12] The sensitivity is limited by the low atomic number (Z) of SiO_x, used as a gate dielectric, which leads to low photoelectric radiation cross-section and, therefore, low absorption. Moreover, Si-based RADFETs are intrinsically rigid and small area devices, hindering concepts as flexible arrays of dosimeters conformable to large, non-flat areas.

Recently, we presented novel flexible Radiation sensitive OXide Field Effect Transistors (ROXFETs).[13,14] ROXFETs are made with high mobility amorphous indium–gallium–zinc oxide (IGZO) semiconductors. IGZO shows stable transport properties even under increased ionizing radiation doses [TID > 400 krad(Si)][15,16] and is

© Author(s) 2024

compatible with large area and low cost fabrication methods. The possibility of producing devices on flexible substrates is a desirable property for wearable detectors with shapes conformal to the human body. Furthermore, amorphous IGZO can be deposited on a wide range of different materials forming the gate dielectric layer, enabling high radiation sensitivity in ROXFET thanks to the combination of high permittivity (κ) and high atomic number oxides.[17] Such dielectric properties are desirable as the high dielectric constant guarantees a strong field effect,[18] even with a thick dielectric layer needed to increase radiation absorption. Simultaneously, the high Z enables a large photoelectric radiation cross-section,[19] resulting in high sensitivity for the device.

Tantalum oxide (Ta_2O_5) has κ ~26 and a high amount of heavy Ta atoms (Z_{Ta} = 73), so it fulfills both requirements. However, as with many high-κ materials, it presents some drawbacks, such as increased parasitic capacitance and low energy. To mitigate these drawbacks, which cause increased gate leakage currents, various strategies have been proposed,[20–23] for example, adding one or more layers of a very large bandgap material. In ROXFETs, we implemented this strategy using either silicon oxide SiO_2 (E_g ~9 eV) or aluminum oxide Al_2O_3 (E_g ~8 eV) layers.

The first reported ROXFET devices[13] were made of a sputtered multi-layer dielectric composed of alternating layers of Ta_2O_5/SiO_2 and SiO_2, and exhibited a sensitivity of (3.4 ± 0.2) V/Gy at 35 keVp (molybdenum source). We demonstrated that the device is suitable for passive radio frequency readout, which allows low-cost, real-time, wireless reading. It was shown that the positive ionization charge accumulation leading to the V_{th} shift was located in the bulk dielectric by studying the sensitivity as a function of the dielectric thickness. However, only one multi-layer dielectric structure was studied, lacking a complete understanding of the effect of the dielectric structure and the implications of the multiple layers on sensitivity. Moreover, the yield of the device fabrication needed to be improved, as the major issue identified was the inhomogeneities of the sputtered multicomponent dielectric film.

Here, we investigate the working principle of ROXFETs presenting a systematic study of the effect of single and multi-layer gate dielectrics to unravel the radiation-induced charge accumulation mechanisms and we identify the best-performing configuration, achieving a sensitivity one order of magnitude higher than the first reported ROXFETs and commercial RADFETs. To support and understand our new findings, we develop a physical model that investigates energetic band alignment among the device layers to explain radiation-induced charge accumulation and recombination mechanisms. Moreover, we implement a new fabrication procedure where the gate dielectric is deposited by atomic layer deposition (ALD) to enhance the uniformity and the insulating properties of the films.[24] The new procedure demonstrates a high fabrication yield with repeatable transistor properties, assuring the possibility of industrial scalability.

RESULTS

Our study aims to investigate and identify the physical processes involved in determining the sensitivity of ROXFET devices, aiming to reliably control and tune detector parameters. The devices are thin-film transistors with a bottom-gate and top-contact geometry [Fig. 1(a)].[25] All the layers are patterned using 365 nm UV

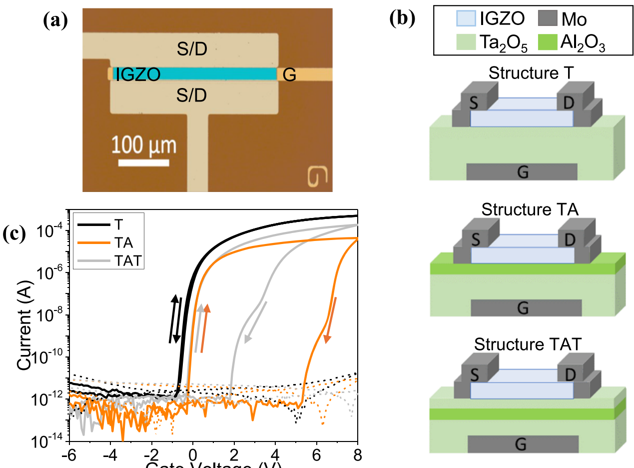

FIG. 1. (a) Optical micrograph showing the active transistor channel of ROXFET. (b) Scheme showing the structure of the investigated transistor configurations with systematic variation in gate dielectric. (c) Transistor transfer curves of samples with the three studied structures. The solid lines represent the drain current, while the dashed lines represent the gate current.

photolithography and etched through reactive ion etching (dielectric) or lift-off (gate electrode, semiconductor, and source–drain electrodes). The electrodes are made of 60 nm of molybdenum deposited by magnetron sputtering. The gate dielectric layer (100 nm total) is deposited by thermal ALD in different compositions, as shown in Fig. 1(b). Structure T is made of a single layer of Ta_2O_5 (100 nm), TA is a bi-layer Ta_2O_5 (80 nm) and Al_2O_3 (20 nm) structure, and TAT is a tri-layer structure made of Ta_2O_5–Al_2O_3–Ta_2O_5 (70–20–10 nm). The ALD process was carried out with a growth rate per cycle of 1.1654 Å/cycle for Al_2O_3 and 0.556 Å/cycle for Ta_2O_5, as determined by stylus profilometry. The semiconducting layer is made of 60 nm IGZO deposited by magnetron sputtering with a ratio of 2.5:1.2:1 for In:Ga:Zn. The channel width and length are W = 320 μm and L = 20 μm, respectively. The devices are annealed in air at 180 °C after the semiconductor layer deposition and at the end of the fabrication.

The typical transfer characteristics in the saturation regime of the Thin-Film Transistors (TFTs) for the three investigated structures are shown in Fig. 1(c). Table I compares the turn-on voltage V_{on}, the mobility μ_{sat}, the subthreshold swing S, and the on/off ratio I_{on}/I_{off} in the three studied structures, extracted from the rising part of the transfer curve and averaged among six devices per structure.

TABLE I. Figures of merit of the studied structures extracted from the transfer characteristics.

Structure	V_{on} (V)	μ_{sat} (cm^2/Vs)	S (V/decade)	I_{on}/I_{off} (decades)
T	−1.2 ± 0.3	7.8 ± 1.9	0.12 ± 0.03	6.3 ± 0.6
TA	−0.62 ± 0.13	7.2 ± 1.4	0.099 ± 0.014	5.2 ± 0.9
TAT	−0.71 ± 0.11	7.2 ± 0.8	0.14 ± 0.06	5.8 ± 1.1

06 March 2024 11:31:13

© Author(s) 2024

Despite the different dielectric compositions, the three configurations show comparable values for all considered parameters. All the devices showed high mobility, a low subthreshold swing, and a high on–off ratio, compatible with typical values of high mobility amorphous oxide semiconductor TFTs.[26] The turn-on voltage is small, thus allowing low voltage operation. The leakage gate current is below 20 pA for all devices for a gate field of 0.8 MV/cm, indicating very good insulating properties of the dielectric structures, considering the low-temperature fabrication process. Configuration *T* has a slightly larger on–off ratio due to the higher dielectric permittivity of Ta_2O_5 compared to Al_2O_3. The same configuration also shows a lower turn-on voltage, which is attributed to a slightly altered interfacial dipole and a related change in flat band voltage.[27] The devices where an Al_2O_3 layer is present show non-negligible hysteresis, which is absent in structure T, where only Ta_2O_5 is present. Structure TA has the biggest hysteresis, which suggests that the hysteresis is due to static charges present at the Al_2O_3 interface. To nullify the impact of hysteresis in the detection mechanism, we used a conditioning procedure for the devices and a dedicated reading cycle that will be later described in detail.

The gate capacitances were measured at 100 kHz using metal–insulator–metal structures fabricated in parallel on the same substrate, obtaining c_T = 203 ± 12 nF/cm^2, c_{TA} = 162 ± 17 nF/cm^2, and c_{TAT} = 154 ± 10 nF/cm^2. The extracted dielectric relative permittivity κ_T = 22.9 ± 1.4 is compatible with the expected Ta_2O_5 permittivity and is higher than κ_{TA} = 18.2 ± 1.9 and κ_{TAT} = 17.4 ± 1.1, which are compatible within experimental accuracy, as the thickness ratio of Ta_2O_5 and Al_2O_3 in the two structures is kept constant.

The effects of x-ray photons were investigated using a tungsten target x-ray tube at 60 kVp of accelerating voltage emitting radiation at a dose rate of 500 μGy/s. It is important to note that here we test a single broad energy spectrum, which makes it difficult to take into account any possible energy dependence of these devices.

First, we tested the effect of conditioning, i.e., the application of a continuous bias to modify the transistor's electrical properties, such as the V_{th} value. Indeed, it is known that in Si-based RADFET, a positive V_{th} creates an internal electric field, which increases the excitonic dissociation, thus increasing internal charge accumulation.[28,29] We achieved a positive threshold voltage in

06 March 2024 11:31:13

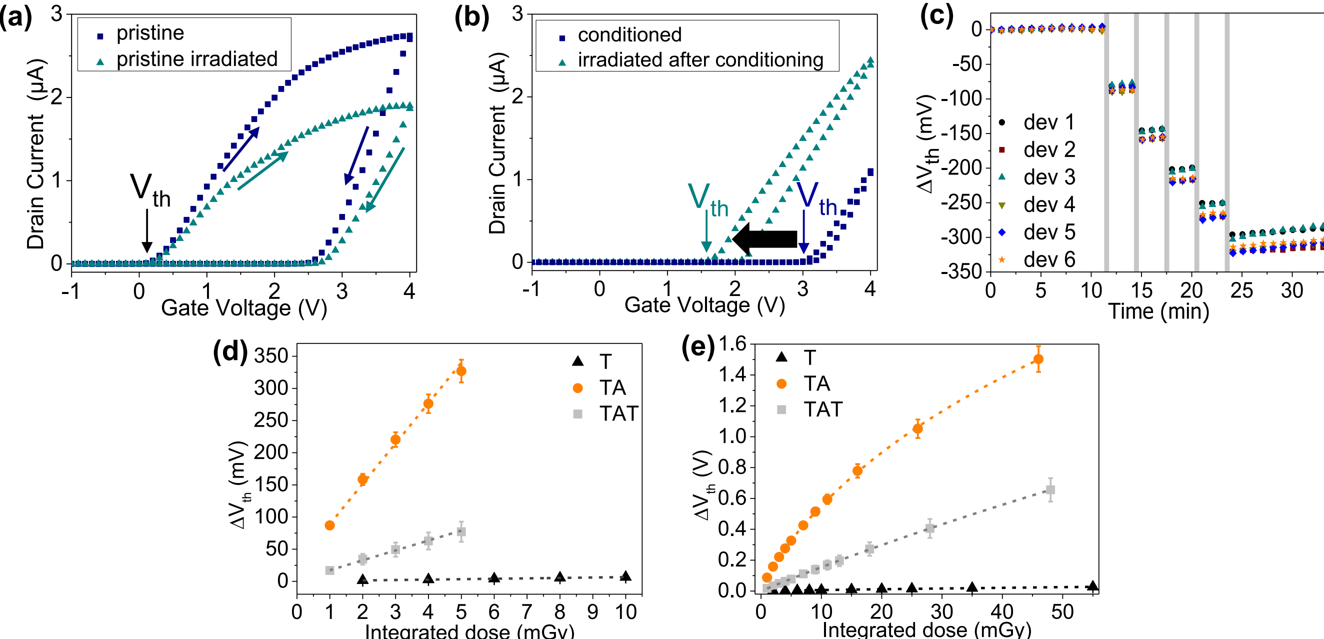

FIG. 2. Transfer characteristic of structure TA before and after 50 mGy irradiation for (a) a pristine device and (b) a conditioned device. (c) Shift of V_{th} during irradiation in six devices with structure *TA*; each irradiation (vertical gray line) corresponds to a total dose of 1 mGy. (d) Total ΔV_{th} as a function of integrated dose with the linear fit (dashed line) performed to extract the sensitivity. The experimental points are obtained by averaging the ΔV_{th} over six devices per structure. (e) Saturation of ΔV_{th} in the studied structures, fitted with Eq. (1) (dashed line).

© Author(s) 2024

ROXFET through device conditioning. All the devices were conditioned by applying 3 V for 5 min to the gate electrode while leaving the source and drain grounded, resulting in a final value of $V_{th}{}^{T}$ = (0.29 ± 0.03) V, $V_{th}{}^{TA}$ = (2.97 ± 0.16) V, and $V_{th}{}^{TAT}$ = (1.3 ± 0.2) V. The threshold voltages were extracted by performing transfer characteristics (V_D = 0.1 V, V_G = [-2; 4] V) over a very short measurement interval (6 ms). In this way, the transfer measurement did not cause any additional bias stress effects on the transistor comparable to the conditioning procedure, i.e., there was no change in transistor parameters during the reading procedure. From the transfer curves, we extracted the threshold voltage by linear fit of the I_D–V_G plot. The higher threshold voltage in ROXFET structure *TA* guarantees higher dissociation ability compared to the other structures, even when the devices are operated in passive mode. The conditioning effect was tested by performing an irradiation of 50 mGy on a pristine device [Fig. 2(a)] and on a conditioned one [Fig. 2(b)]. The pristine one shows a negligible ΔV_{th} but a decrease in mobility ($\Delta\mu$ = 1.17 ± 0.08 cm^2/Vs). The conditioned device shows a shift in threshold voltage (ΔV = 1.44 ± 0.18 V) and no change in mobility. Traditionally, in silicon-based RADFETs, charges generated in the bulk dielectric are associated with threshold shift, while the creation of interface charges is associated with a change in both the threshold voltage and the mobility due to carrier scattering.[30] Therefore, in the pristine device, where we see a change in mobility, we can assume that there is a contribution coming from interfacial charges. On the other hand, in the conditioned devices, the radiation induced charge accumulation in the bulk dielectric is dominant thanks to enhanced excitonic dissociation caused by the built-in electric field. The dominance of bulk charges in the sensitivity of ROXFET was also observed in ROXFET with sputtered dielectric, where the sensitivity depends quadratically on the dielectric thickness.[13] It is also visible that the conditioning procedure nullifies the hysteresis even when performing slow transfer characteristics. Indeed, we can assume that the conditioning procedure removes static interfacial charges present in pristine devices that cause mobility and threshold instability. Therefore, as the devices are used only after the conditioning procedure, the hysteresis is relevant to the detection mechanism.

We follow the V_{th} over time, performing one fast transfer characteristic (V_D = 0.1 V, V_G = [−2; 4] V, lasting 6 ms, as described above) per minute. Between reading cycles, all the electrodes were kept grounded, and the devices were exposed to five irradiation steps of 1 mGy each (2 mGy for structure *T*). Figure 2(c) shows the ΔV_{th} over time occurring in six devices of a batch with structure *TA* during these irradiations. Notably, the plot shows very repeatable behavior among all devices, demonstrating a high fabrication yield. It is also visible that V_{th} is stable before irradiation and shows a slow recovery in timescales much longer than their x-ray response. The stable threshold voltage during the first 10 min of measurements proves that the reading procedure does not perturb the conditioned state of the detector. All structures present a negative V_{th} shift under x rays. As the devices work as integrators of radiation-induced charges, the x-ray sensitivity of the three structures is extracted by a linear fit of the average ΔV_{th} as a function of the integrated dose. Figure 2(d) shows the linear trend of the V_{th} shift in the three structures averaged on six devices per structure. The obtained sensitivities are S_T = (0.65 ± 0.02) V/Gy, S_{TA} = (63 ± 2) V/Gy, and S_{TAT} = (15.4 ± 0.5) V/Gy. Structure *TA* shows an order of magnitude increase in sensitivity compared to structure *T*, while structure *TAT* shows an intermediate sensitivity. These values should be compared with the one previously reported by our group for ROXFETs with a sputtered gate dielectric composed of seven layers of alternated Ta_2O_5/SiO_2 and SiO_2 for a total of 400 nm (*TS* structure).[13] The sensitivity of *TS* devices was S_{TS}= (3.4 ± 0.2) V/Gy. Interestingly, the *TS* configuration has lower sensitivity than bilayer *TA* and tri-layer *TAT*, despite the higher layer number and bigger thickness. A possible explanation will be presented later in the article.

Structure *TA* has very high sensitivity, resulting in a low limit of detection, *LOD* = (55 ± 3) μGy, comparable to commercial dosimeter values.[31] However, the large voltage shift generates a deviation from linearity already at 5 mGy. Structure *TAT* and *T* have smaller sensitivity, but their linear behavior with integrated dose extends above 50 mGy. The ΔV_{th} saturation with integrated dose [Fig. 2(e)] can be described following the formula proposed by Ristić *et al.*:[32]

$$\Delta V_{th} = V_{sat} - \frac{V_{sat}}{1 - aD^b}, \tag{1}$$

where D is the integrated dose and V_{sat} is the saturation voltage, while a and b are fit parameters, which are summarized in Table II for the studied structures.

To summarize, the bilayer structure (*TA*) is the best performing detector at low doses, while single-layer (*T*) and tri-layer (*TAT*) structures could be best employed for applications requiring high doses of irradiation and a large operative range. In the detection mechanism, we assume that in ROXFET, the charge accumulation happens in the gate dielectric. Recently, we proved our assumption with local electrostatic measurements using Kelvin Probe Force Microscopy (KPFM) performed on the semiconductor layer of a device with structure *TA* before and after x-ray irradiation.[33] The measurements demonstrated that the amount of doping due to oxygen vacancies remains unaltered during irradiation. Similarly, the band structure remains constant. Instead, the ΔV_{th} is directly related to an offset in flat band potential caused by static charge deposited in the gate dielectric.

To understand the broad range of sensitivity brought about by single, bi-, and tri-layer structures (*T*, *TA*, and *TAT*), we must consider both external quantum efficiency (i.e., the ratio of the radiation-generated charges to the number of impinging photons on the sample) and internal charge accumulation and recombination mechanisms. The radiation absorption is calculated from Beer–Lambert's law, using the linear attenuation coefficient of the oxides at the simulated average beam energy. Among the measured structures, *T* has the highest external quantum efficiency (equal to 0.3%) thanks to the highest amount of heavy Ta atoms within the full

TABLE II. Saturation parameters for the three structures extracted by fitting the ΔV_{th} as a function of the integrated dose with Eq. (1).

Structure	V_{sat} (V)	a (μGy^{-1})	b
T	180 ± 40	−4.4 ± 0.8	0.93 ± 0.01
TA	4700 ± 200	−20.0 ± 1.2	0.86 ± 0.01
TAT	8500 ± 400	−2.0 ± 0.8	0.10 ± 0.01

06 March 2024 11:31:13

© Author(s) 2024

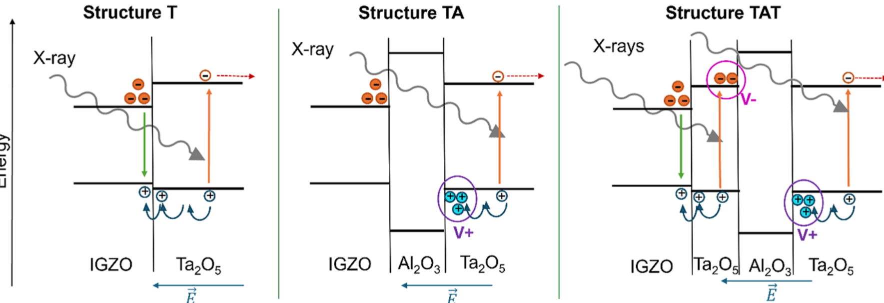

FIG. 3. Energetic scheme of the studied structures and the behavior of radiation-induced charges of (a) structure *T* with the lowest sensitivity, (b) structure *TA* with the highest sensitivity, and (c) structure *TAT* with intermediate sensitivity.

dielectric volume, which leads to the highest absorption and, therefore, the highest amount of radiation-generated charge. Nonetheless, the scenario changes completely considering the internal processes of charge accumulation and recombination. Upon x-ray exposure, electron–hole pairs are generated inside the dielectric. Here, we consider that most of the radiation-induced charges are generated in the Ta_2O_5 layer due to its higher Z and thickness (80 nm total in both multi-layer structures), while the ones in the 20 nm Al_2O_3 layer are negligible, contributing only 0.4% of the total external quantum efficiency. The charge separation of the ionization excitons is enhanced by the electric fields present inside the gate dielectric. Electrons, driven by the electric field, are quickly collected at the metallic gate thanks to their high mobility. On the other hand, the holes have lower mobility, and they slowly drift toward the semiconductor interface. If they manage to reach it, the positive charges can easily cross the interface due to the favorable valence band alignment of IGZO and Ta_2O_5, and they recombine with electrons in the IGZO channel. On the contrary, whenever an Al_2O_3 layer is found between the Ta_2O_5 and the IGZO layers, its large bandgap blocks the holes in the Ta_2O_5 layer, where they accumulate, generating an additional fixed positive potential. In the transistors, this additional positive potential results in the channel opening at more negative voltages, which corresponds to the measured ΔV_{th} toward negative values proportional to the irradiated dose. The proposed mechanism explains both the low sensitivity of structure *T* [Fig. 3(a)], where most of the positive radiation induced charges recombine at the IGZO interface, and the high sensitivity of structure *TA* [Fig. 3(b)], where most of the positive charges accumulate in the Ta_2O_5 layer blocked by the Al_2O_3 layer. The intermediate sensitivity of structure TAT [Fig. 3(c)] can be explained as well by separating a bilayer structure similar to *TA* formed by the Ta_2O_5 layer in contact with the gate and the Al_2O_3 layer and a monolayer structure formed by the Ta_2O_5 layer in contact with the semiconductor. The bilayer contributes with an additional fixed positive voltage (V^+) as for structure *TA*. On the other hand, the additional Ta_2O_5 layer behaves similarly to how described for structure *T*, with the exception that the photogenerated excess electrons are not able to exit from the dielectric due to the blocking layer of Al_2O_3, resulting in a negative charge contribution. The photogenerated holes, instead, are still pushed by the electric field toward the electron-rich IGZO, where they can recombine. Therefore, the accumulation of negative charges in this layer results in a fixed negative voltage contribution (V^-), which attenuates the contribution of the positive charges trapped in the other Ta_2O_5 layer (V^+). As a result, the optimized structure is a bilayer where no charge shielding happens. In this view, the charge shielding mechanism lowers the sensitivity of complex multi-layered structures, which could also explain the low sensitivity of structure *TS* made of seven layers, where the SiO_2 layer had a similar function to the Al_2O_3 layer described here.

CONCLUSIONS

In summary, we developed a novel fabrication procedure for ROXFET personal dosimeters, consisting of IGZO-based TFTs with ALD deposited dielectric layers made of Ta_2O_5 and Al_2O_3, allowing for high reproducibility and fabrication yield. The devices can be operated in air in passive mode after a short conditioning of 5 min at 3 V. ROXFET devices with bilayer structure (*TA*) show an outstanding sensitivity of S_{TA} = (63 ± 2) V/Gy at 60 kVp, the highest among integrating solid-state dosimeters, to our knowledge. We demonstrate that the conditioning process, which induces an electric field across the dielectric, enhances excitonic dissociation and, over time, results in the accumulation of radiation-induced charges in the bulk dielectric. Moreover, the performance comparison among three different dielectric structures (*T*, *TA*, and *TAT*) allows us to describe and model the process of generation, accumulation, and recombination of charge inside the dielectric. We investigate and discuss the physical processes influencing the device sensitivity and attribute the excellent performance of structures TA both to the effective conditioning and to the alignment in the energetic band structure. Indeed, the suggested optimal dielectric structure is composed of a highly absorbing layer (Ta_2O_5) combined with a large bandgap layer (Al_2O_3) between the Ta_2O_5 and the semiconducting layer. Its role is to confine the radiation induced positive charges in the absorbing layer, preventing their recombination with the IGZO channel electrons. To conclude, the new fabrication procedure with an ALD deposited dielectric and the modeling of the radiation-induced charge accumulation and recombination described in this article allow the realization of a new reliable and efficient design of ROXFETs.

06 March 2024 11:31:13

© Author(s) 2024

ACKNOWLEDGMENTS

The authors acknowledge the funding by the EU—NextGenerationEU—with funds made available by the National Recovery and Resilience Plan (NRRP) Mission 4, Component 1, Investment 4.1 (MD 351/2022)—NRRP Research. This work also received funding from the European Community's Horizon Europe program (ERC-POC FLETRAD, Grant Agreement No. 101082283) and from National Funds through the FCT —Fundação para a Ciência e a Tecnologia, I.P.), Project Nos. LA/P/0037/2020, UIDP/50025/2020, and UIDB/50025/2020 of the Institute of Nanostructures, Nanomodelling and Nanofabrication—i3N. We would also like to acknowledge the Portuguese Foundation for Science and Technology, under the scope of doctoral Grant Nos. DFA/BD/8335/2020 and 2022.09516.BD, for the support.

AUTHOR DECLARATIONS

Conflict of Interest

T.C., P.B., and B.F. are inventors on an international patent application related in part to this work (serial no. PCT/IT2017/000050, priority date: November 14, 2016). The authors have no conflicts to disclose.

Author Contributions

Camilla Bordoni: Data curation (lead), Investigation (lead); Writing – original draft (lead); Writing – review & editing (equal). **Andrea Ciavatti**: Methodology (lead); Investigation (equal); Writing – review & editing (lead). **Mariana Cortinhal**: Investigation (equal); Writing – review & editing (equal). **Maria Pereira:** Investigation (equal); Writing – review & editing (equal). **Tobias Cramer**: Conceptualization (equal); Funding acquisition (equal); Supervision (equal); Writing – review & editing (equal). **Pedro Barquinha**: Conceptualization (equal); Funding acquisition (equal); Project administration (equal); Resources (lead); Supervision (equal); Writing – review & editing (equal). **Beatrice Fraboni**: Conceptualization (equal); Funding acquisition (equal); Project administration (equal); Resources (equal); Supervision (lead); Writing – review & editing (equal).

DATA AVAILABILITY

The data that support the findings of this study are available from the corresponding author upon reasonable request.

REFERENCES

[1]F. Vanhavere *et al.*, "An overview on extremity dosimetry in medical applications," Radiat. Prot. Dosim. **129**, 350–355 (2008).

[2]J. A. Caffrey and D. M. Hamby, "A review of instruments and methods for dosimetry in space," Adv. Space Res. **47**, 563–574 (2011).

[3]W. L. Jong *et al.*, "In vivo skin dose measurement using MOSkin detectors in tangential breast radiotherapy," Physica Med. **32**, 1466–1474 (2016).

[4]S. Dhanekar and K. Rangra, "Wearable dosimeters for medical and defence applications: A state of the art review," Adv. Mater. Technol. **6**, 2000895 (2021).

[5]M. C. Müller *et al.*, "Real-time dosimetry reduces radiation exposure of orthopaedic surgeons," Orthopaedics Traumatol.: Surg. Res. **100**, 947–951 (2014).

[6]I. Fratelli *et al.*, "Trap states ruling photoconductive gain in tissue-equivalent, printed organic X-ray detectors," Adv. Mater. Technol. **8**, 2200769 (2023).

[7]M. M. Pejović and S. M. Pejović, "P-channel MOSFET as ionizing radiation detector," Appl. Radiat. Isot. **196**, 110730 (2023).

[8]T. R. Oldham and F. B. McLean, "Total ionizing dose effects in MOS oxides and devices," IEEE Trans. Nucl. Sci. **50**, 483–499 (2003).

[9]K. F. Galloway and R. D. Schrimpf, "MOS device degradation due to total dose ionizing radiation in the natural space environment: A review," Microelectron. J. **21**, 67–81 (1990).

[10]A. Karmakar, J. Wang, J. Prinzie, V. De Smedt, and P. Leroux, "A review of semiconductor based ionising radiation sensors used in harsh radiation environments and their applications," Radiation **1**, 194–217 (2021).

[11]W. L. Jong *et al.*, "Characterization of MOSkin detector for in vivo skin dose measurement during megavoltage radiotherapy," J. Appl. Clin. Med. Phys. **15**, 120 (2014).

[12]A. B Rosenfeld, "MOSFET dosimetry on modern radiation oncology modalities," Radiat. Prot. Dosim. **101**, 393–398 (2002).

[13]T. Cramer *et al.*, "Passive radiofrequency x-ray dosimeter tag based on flexible radiation-sensitive oxide field-effect transistor," Sci. Adv. **4**, eaat1825 (2018).

[14]R. F. D. P. Martins, P. M. C. Barquinha, E. M. C. Fortunato, T. Cramer, and B. Fraboni, "Sensitive field effect device and manufacturing method thereof," U.S. Patent No. 11360044 B2 (2022).

[15]T. Cramer *et al.*, "Radiation-tolerant flexible large-area electronics based on oxide semiconductors," Adv. Electron. Mater. **2**, 1500489 (2016).

[16]D. Ho *et al.*, "In situ radiation hardness study of amorphous Zn–in–Sn–O thin-film transistors with structural plasticity and defect tolerance," ACS Appl. Mater. Interfaces **15**, 33751–33762 (2023).

[17]P. Barquinha *et al.*, "Low-temperature sputtered mixtures of high-κ and high bandgap dielectrics for GIZO TFTs," J. Soc. Inf. Disp. **18**, 762–772 (2010).

[18]A. Liu, H. Zhu, H. Sun, Y. Xu, and Y.-Y. Noh, "Solution processed metal oxide high-κ dielectrics for emerging transistors and circuits," Adv. Mater. **30**, 1706364 (2018).

[19]L. Basiricò, A. Ciavatti, and B. Fraboni, "Solution-grown organic and perovskite X-ray detectors: A new paradigm for the direct detection of ionizing radiation," Adv. Mater. Technol. **6**, 2000475 (2021).

[20]J.-H. Lee, H.-S. Park, J.-H. Jeon, and M.-K. Han, "Suppression of TFT leakage current effect on active matrix displays by employing a new circular switch," Solid-State Electron. **52**, 467–472 (2008).

[21]Y.-H. Liang, S. Kumaran, M. Zharnikov, and Y. Tai, "Reduction of leakage current in amorphous oxide-semiconductor top-gated thin film transistors by interface engineering with dipolar self-assembled monolayers," Appl. Surf. Sci. **569**, 151029 (2021).

[22]W. Jeon, "Recent advances in the understanding of high-*k* dielectric materials deposited by atomic layer deposition for dynamic random-access memory capacitor applications," J. Mater. Res. **35**, 775–794 (2020).

[23]N. Jain, S. K. Sharma, R. Kumawat, A. Jain, and S. Lakhawat, "Influence of high-*k* dielectric material on the electrical performance of a-IGZO Thin Film Transistor," Mater. Today: Proc. **66**, 3553–3558 (2022).

[24]P. Ma *et al.*, "Low voltage operation of IGZO thin film transistors enabled by ultrathin Al_2O_3 gate dielectric," Appl. Phys. Lett. **112**, 023501 (2018).

[25]J. Martins *et al.*, "Ta_2O_5/SiO_2 multicomponent dielectrics for amorphous oxide TFTs," Electron. Mater. **2**, 1–16 (2021).

[26]E. Fortunato, P. Barquinha, and R. Martins, "Oxide semiconductor thin-film transistors: A review of recent advances," Adv. Mater. **24**, 2945–2986 (2012).

[27]G. Z. Geng *et al.*, "Improved performance of InGaZnO thin-film transistors with Ta_2O_5/Al_2O_3 stack deposited using pulsed laser deposition," Curr. Appl. Phys. **14**, S2–S6 (2014).

06 March 2024 11:31:13

© Author(s) 2024

[28]G. Sarrabayrouse and S. Siskos, "Low dose measurement with thick gate oxide MOSFETs," Radiat. Phys. Chem. **81**, 339–344 (2012).
[29]A. Holmes-Siedle, L. Adams, and G. Ensell, "MOS dosimeters-improvement of responsivity," in *RADECS 91 First European Conference on Radiation and Its Effects on Devices and Systems* (IEEE, 1991), pp. 65–69.
[30]G. Sarrabayrouse and F. Gessinn, "Thick oxide MOS transistors for ionizing radiation dose measurement," Radioprotection **29**, 557–572 (1994).
[31]Tecnorad dosimeter Green Film, https://www.tecnorad.it/en/prodotto/dosimetria/green-film/ (accessed 06 July 2023.
[32]G. S. Ristić, M. Andjelković, and A. B. Jakšić, "The behavior of fixed and switching oxide traps of RADFETs during irradiation up to high absorbed doses," Appl. Radiat. Isot. **102**, 29–34 (2015).
[33]L. Fabbri *et al.*, "Accurate determination of band tail properties in amorphous semiconductor thin film with Kelvin probe force microscopy," APL Mater. **11**, 061123 (2023).

06 March 2024 11:31:13

© Author(s) 2024